Philosophical Magazine
Publication details, including instructions for authors and subscription information:
http://www.tandfonline.com/loi/tphm20

Evidence of grain boundary dislocation step motion associated to shear-coupled grain boundary migration

A. Rajabzadeh [a], M. Legros [a], N. Combe [a b], F. Mompiou [a] & D.A. Molodov [c]

[a] CEMES-CNRS, Université de Toulouse, 29 rue J. Marvig, 31055, Toulouse, France

[b] Université de Toulouse, UPS, 31055, Toulouse, France

[c] Institute of Physical Metallurgy and Metal Physics, RWTH Aachen University, 52056, Aachen, Germany

Version of record first published: 01 Feb 2013.

To cite this article: A. Rajabzadeh , M. Legros , N. Combe , F. Mompiou & D.A. Molodov (2013): Evidence of grain boundary dislocation step motion associated to shear-coupled grain boundary migration, Philosophical Magazine, DOI:10.1080/14786435.2012.760760

To link to this article: http://dx.doi.org/10.1080/14786435.2012.760760

Philosophical Magazine, 2013
http://dx.doi.org/10.1080/14786435.2012.760760

Taylor & Francis
Taylor & Francis Group

Evidence of grain boundary dislocation step motion associated to shear-coupled grain boundary migration

A. Rajabzadeh[a], M. Legros[a], N. Combe[a,b], F. Mompiou[a]* and D.A. Molodov[c]

[a] *CEMES-CNRS and Université de Toulouse, 29 rue J. Marvig, Toulouse 31055, France;* [b] *Université de Toulouse, UPS, Toulouse 31055, France;* [c] *Institute of Physical Metallurgy and Metal Physics, RWTH Aachen University, Aachen 52056, Germany*

(*Received 4 September 2012; final version received 14 December 2012*)

The present work reports dynamical observations of the grain boundary (GB)-mediated plasticity during *in situ* transmission electron microscopy straining experiments at moderate temperature (400°C) both in a 76.4° ⟨0 0 1⟩ bicrystalline and a polycrystalline Al sample. We show that the GB migration occurs by the lateral motion of elementary GB dislocation steps. The accumulation of GB dislocation steps eventually form macro-steps. This observation agrees with the idea that GB dislocation steps generally operate in high angle GBs similarly as in twinning or martensitic transformations. The coupling factor, i.e. the strain produced by the motion of the steps was measured using fiducial markers and image correlation. The migration process involves different types of GB dislocation steps, producing different amounts of strain both parallel (coupling factor) and perpendicular to the GB plane.

Keywords: grain boundary; shear-migration coupling; dislocation; step

1. Introduction

Dislocations are the easiest vector of plastic deformation over a wide range of stress and temperature for many crystalline and polycrystalline materials, but there are several evidence that grain boundaries (GBs) can also carry out a significant amount of permanent deformation through migration [1]. GB migrations can occur at large speed under stress in nanometer-sized polycrystals [2,3]. It can also produce strain as shown in experiments with low angle GBs [4,5], low Σ coincident high angle GBs (for instance during twinning) [6], near coincident GBs [7–9] and as found more recently for arbitrary high angle GBs [10–13]. The GB migrations hence present some similarities with the motion of interfaces associated with a strain as seen in twinning or in martensitic phase transformation [14]. In the literature, two main GB motion mechanisms have been reported [15–17]: the coupled motion and the sliding. A recent Molecular Dynamics study showed that in pure nanocrystalline metals, sliding was rapidly hindered and overcome by coupling [18]. Sliding will not then be considered in the following. Coupling, on which this study focuses, is only possible for pure tilt GB [16].

Figure 1 reports a sketch of the coupling between the GB motion and the strain for a pure tilt GB with a rotation axis pointing out of the plane of the image. Under a shear stress τ,

*Corresponding author. Email: mompiou@cemes.fr

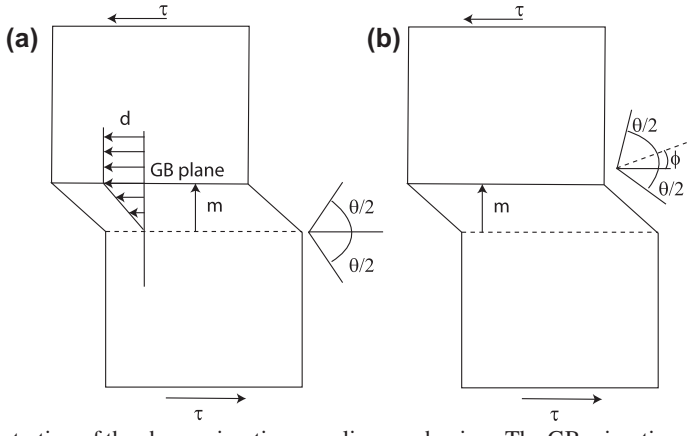

Figure 1. Illustration of the shear-migration coupling mechanism. The GB migration over a distance m under a shear stress τ parallel to the GB plane produces a shear displacement d. The coupling factor $\beta_{\parallel} = d/m$ is thought to be related to the misorientation angle θ and to the symmetrical (a) or asymmetrical (b) nature of the GB, but the relation between these different parameters depends on the model considered.

the GB migrates from position (i) to (f) over a distance m. This migration produces a displacement d parallel to the GB plane i.e. a shear displacement. The shear strain is characterized by the coupling factor $\beta_{\parallel} = d/m$. The subscript $\parallel$ is used to indicate that the strain is parallel to the GB plane. At variance to intragranular dislocations which have well known Burgers vectors, the coupling factor of a migrating GB is not *a priori* known. The literature suggests that it mainly depends on the misorientation θ and on the nature of the GB which can be symmetrical (Figure 1(a), $\phi = 0$) or asymmetrical (Figure 1(b), $\phi \neq 0$) . In this study, we will refer to "coupling mode" as a coupled motion of the GB with a given coupling factor.

Several theoretical studies have been proposed to account for this coupling, all of them being purely geometrical [16,17,19–21]. They are schematically depicted in Figure 2 and described below.

Read and Shockley [22] describe the migration of a pure tilt symmetrical GB by the motion of the primary intrinsic lattice dislocations perpendicular to the GB plane (Figure 2(a)). This theory initially applies for low-angle GBs but has been extended to high-angle symmetrical and asymmetrical GBs [16,17,23]. This latter case involves the cooperative gliding of two sets of dislocation families of Burgers vectors $\vec{b}_1$ and $\vec{b}_2$ (Figure 2(b)). In this theory, the coupling factor depends only on the density of the dislocations which, according to the Frank–Bilby equation, varies continuously with the misorientation angle (θ). As a consequence, the coupling factor is a continuous function of θ. For a [100] tilt GB in a FCC lattice, this theory predicts two coupling modes referred as $\langle 1\,0\,0 \rangle$ and $\langle 1\,1\,0 \rangle$ modes, in good agreements with molecular dynamics simulations [17,24]. Note that these latter simulations have reported both an overall motion of the GB and the nucleation and growth mechanism initiated by the formation of a relatively small area over which the GB has advanced. This nucleus is defined by the existence of steps along the GB, the disconnections [25].

In the pure shuffling mode [26] (Figure 2(c)), GB migration occurs by the nucleation and lateral displacement of a pure step, i.e. a coherent ledge, perpendicular to the GB plane,

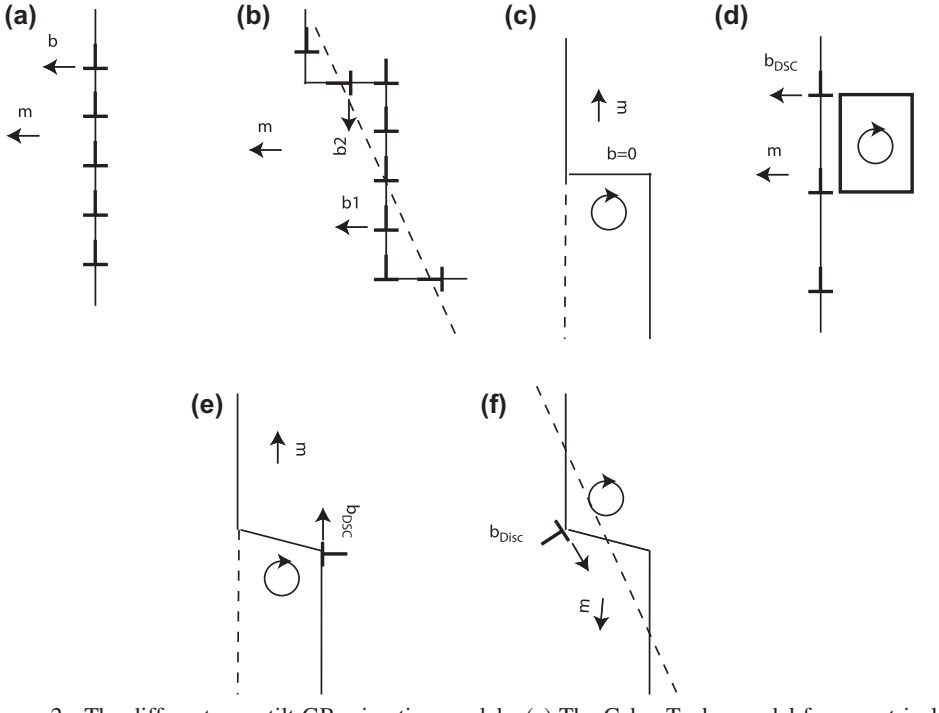

Figure 2. The different pure tilt GB migration models. (a) The Cahn–Taylor model for symetrical GB. (b) The Cahn–Taylor model for asymetrical GB. (c) The pure shuffling model. (d) Combination of pure shuffling and Cahn–Taylor model. (e) The DSC dislocation model. (f) The SMIG model. $\vec{m}$ indicates the direction of motion of the defects of Burgers vector $\vec{b}$. The circular arrow represents atomic shuffling.

which does not produce shear strain. Hirth has however suggested that the pure shuffling mode can be assisted by the applied stress [27]. As the pure step moves laterally (parallel to the direction $\vec{m}$), atoms have to be rearranged by a local shuffling.

Combining these two former models [11], a high angle GB can be described as to be close to a coincident GB, the extra misorientation angle should be accommodated by secondary (DSC) edge dislocations $\vec{b}_{DSC}$ (Figure 2(d)). Accordingly, as discussed in [11], the shear-coupled migration should then operate by i) pure shuffling and ii) the motion of DSC dislocations perpendicular to the GB plane.

This view is completely equivalent to the DSC dislocation theory for coincident GBs [19, 28]. In this theory, the DSC dislocation has a step character and glide parallel to the GB plane while atoms re-arrange in the wake of the step (Figure 2(e)). In the case of a near coincident GB, secondary DSC dislocations which compensate the misorientation are supposed to move perpendicularly to the GB at the same time [8].

More recently, the Shear Migration Geometrical (SMIG) model [20, 29] adopts an approach similar to the geometrical theory of twinning [6] and to the Phenomenological Theory of Martensitic Crystallography [30], which allows the computation of coupling modes for any arbitrary GB. This model relies on the hypothesis that for a given interface plane and misorientation angle, there exists a GB dislocation step, also called disconnection

of a Burgers vector $\vec{b}_{Disc}$ that defines the invariant shear direction (Figure 2(f)). According to Pond et al. [14, 25, 31, 32], this defect is supposed to glide along terraces which follow in average the GB plane. This description, which is particularly suitable for asymmetrical GBs, predicts several coupling modes for a given GB.

To test these theories, both experiments and computer simulations have been performed in the recent years. Several studies [9,12,13] report that the coupling factor depends on the misorientation angle θ between the two adjacent lattices (Figure 1) following the Read–Shockley predictions. Some other recent studies performed on both polycrystalline and bicrystalline specimens report low coupling factors that can be explained by the SMIG model, but not by the Read–Shockley predictions [10, 11, 33]. It has also been shown that shear-coupled migration can occur concomitantly with grain rotation [34].

Interfacial dislocation models, like the SMIG model proposed recently, are expected to capture more easily these variations because it allows a large variety of defects to be responsible of the GB coupling. However, despite the large amount of experimental evidence of shear-coupled GB migration, the hypothesis of dislocation or disconnection motion in the GB as a possible mechanism of shear-coupled migration has still to be demonstrated.

In the current paper, we report *in situ* TEM observations of defects moving along a GB in response to a stress in Aluminium bicrystals and polycrystals. We show that these defects have a step character and produce a shear strain that can be measured. We will first describe some observations of the motion and the nucleation of these defects. We will then measure some characteristics (including the coupling factor) of the displacements associated to the migration of the GB. Finally, we will give some evidence that the collective motion of these defects can explain a more complex shear-migration coupling situation involving three grains.

2. Experimental

Both an Al bicrystal and an Al polycrystal have been considered. The high purity Al bicrystal (99.9995%) with a symmetrical 76.4° ⟨001⟩ tilt boundary was produced by the Bridgman technique. Details of the crystal growth and bicrystal characterization are reported elsewhere [12,13,33–36]. Bicrystalline samples were cut out perpendicularly to the misorientation axis and in a way that the GB plane normal forms a 45° angle with respect to the straining axis. This experimental scheme was also used previously for the macroscopic measurements of stress-induced GB migration in Al bicrystals [12, 13]. It allows a maximum resolved shear stress parallel to the GB plane.

An Al polycrystal with an initial mean grain size of about 800 nm was produced by equal-channel angular pressing. Rectangular samples were fabricated by spark cutting and thinned down by electro-chemical polishing using a methanol solution with 33% of nitric acid at $T = -10$ °C. Gold nanoparticules were deposited at the sample surfaces in order to act as fiducial markers for measuring the deformation.

In situ straining experiments were carried out in a JEOL 2010 microscope operated at 200 kV at ca. 400°C in order to promote GB migration. Such temperature approximately corresponds to 0.7 T_m, with T_m the melting temperature of Al. The experiments consisted of applying an increment of strain and observing the deformation during stress relaxation. GB motion was monitored by means of DVD/HD recording using a 25 fps video rate MEGAVIEW III camera.

3. Results

3.1. *GB shear-coupled migration due to GB dislocation step motion*

3.1.1. *Observation of elementary GB dislocation steps*

Figure 3 shows bright field micrographs taken during a straining experiment with the bicrystalline sample. The GB between grains G_1 and G_2 is seen here edge on, i.e. along the $\langle 0\,0\,1\rangle$ direction. The straining axis (T) is indicated by an arrow in Figure 3(a). A 2 nm height step, labelled s in Figure 3(a) can be clearly seen. Though they do not appear in Figure 3, several other steps of this height have also been observed along the GB. The evaluation of the distribution of the distances between steps is out of the scope of this study.

Under stress, the step has been observed to move over 25 nm along the grain toward the nanoparticle X at a maximum speed of few angstroems per second (Figure 3(b) and (c)): this motion can readily be observed in the video provided as an additional material to this paper. In the meantime, a lattice dislocation, labelled d in Figure 3(b), glides in a {111} plane of G_2: the trace of the glide plane has been reported as $tr.P$ in Figure 3(b). The dislocation d then eventually interacts with the GB dislocation step (Figure 3(d)). The step then remains immobile suggesting that the interaction has led to the formation of a sessile GB dislocation step. The simultaneous motion of the step and the lattice dislocation suggests that the step has a dislocation character, i.e. that it is sensitive to an external applied and/or an elastic strain field due to the presence of the dislocation d in its vicinity. As a consequence, the step is identified as a GB dislocation step i.e. a disconnection.

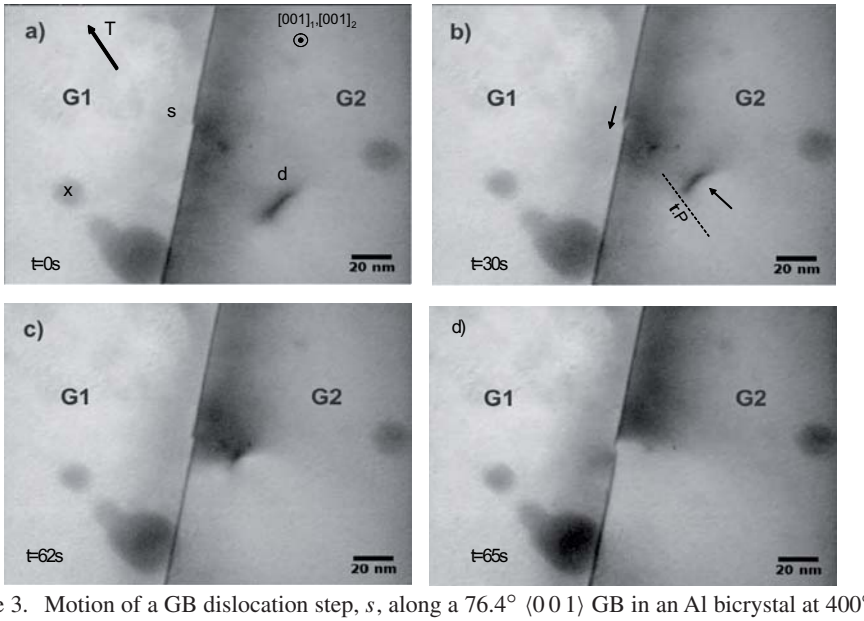

Figure 3. Motion of a GB dislocation step, s, along a 76.4° $\langle 0\,0\,1\rangle$ GB in an Al bicrystal at 400° C. Time and scales are reported on each picture. The straining axis (T) is indicated by an arrow. x is a fixed point.

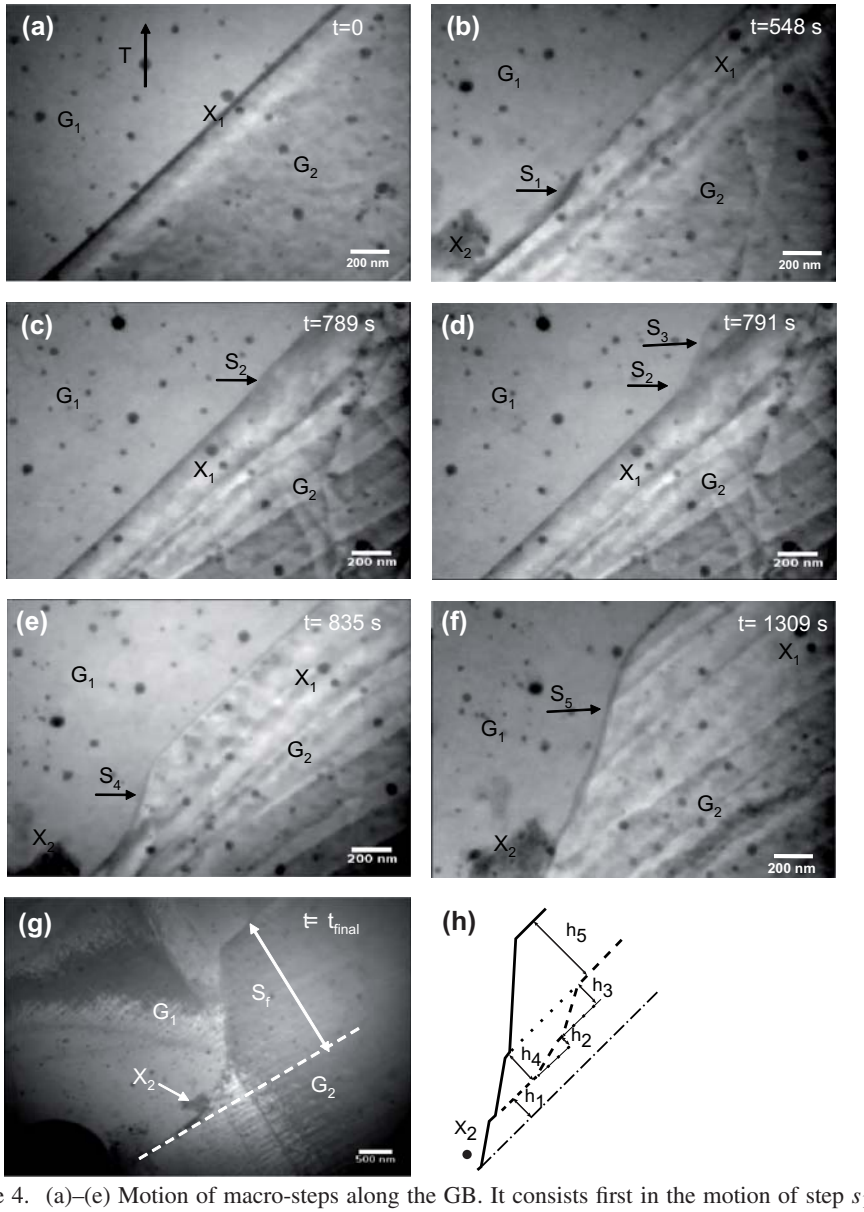

Figure 4. (a)–(e) Motion of macro-steps along the GB. It consists first in the motion of step s_1 (a-b) followed by the motion of s_3 which absorbs the immobile step s_2 (c-d) forming a step s_4 that eventually moves toward X_2 (d-e). (f-g) are configurations after the motion of several other steps. The final step s_f which has largely grown is about $2\mu m$ high. (h) is a sketch of the different steps and their corresponding height.

3.1.2. *Macro-step formation*

Figure 4 reports the results of another straining experiment on the same bicrystal (different sample). The video corresponding to this figure can be seen in the supplementary material section. The initial configuration is shown in Figure 4(a). The straining axis (T) is indicated

by an arrow in Figure 4(a). After 548 s, a first step, labelled s_1 of height h_1=95 nm, moves at a speed of about 4 μm/s along the GB toward the marker X_2 (Figure 4(b)) and eventually stops close to X_2. The step height h_1 is around 50 times the elementary GB dislocation step height, suggesting that this macro-step is composed of elementary steps. Later on, at $t = 789$ s, a second step s_2 of height $h_2 = 50$ nm, initially immobile is observed close to the marker X_1 (Figure 4(c)). Two seconds later, a third step s_3 of height $h_3 = 100$ nm arriving from the thicker area of the sample meets s_2 where it stops (Figure 4(d)). A single step s_4 of height h_4=150 nm is then formed. At $t = 835$s, the step s_4 starts moving rapidly at about 4 μm/s along the GB (Figure 4(e)) before being definitely blocked close to the marker X_2. In the meantime, s_4 absorbs s_1. Simultaneously to the blocking of s_4, a dislocation activity in G_1 is noticed. The motion of one or several other steps eventually occurs leading to the formation of the step s_5 of a height $h_5 = 250$ nm after 1309 s (Figure 4(f)) and finally to a 2 μm high step s_f after several minutes (Figure 4(g)). Note also in Figure 4(g), the large number of slip traces in both grains, indicating that part of the strain is also relaxed by intragranular plasticity.

The blocking of the step s_4 motion is attributed to the presence of a surface defect, most likely an aggregate of nanoparticles that pins the step at the sample surface. In addition, a careful analysis of Figure 4(d) shows that i) the shape of s_2 and s_3 can still be distinguished in the step s_4 and that ii) the height of s_4 is approximately equal to the sum of the heights of the steps s_2 and s_3. Similarly, the profile of the GB in Figure 4(f) can be interpreted as a stack of macro-steps: Figure 4(h) provides a sketch of the four different steps that accumulated to form the macro-step s_f.

From these observations, we concluded that GB migration occurs via the collective motion of elementary steps that progressively stack until forming macro-steps. Indeed, because of the impossibility of passing, faster steps will eventually pile up against immobile or slowest ones while they are temporarily slowed down or blocked, resulting in the slowing down of the migration process.

3.1.3. *Measurements of the coupling factor*

From Figure 4, it is possible to extract and measure some characteristics (including the coupling factor) of the displacements associated to the GB migration. These displacements are deduced from image correlations as previously described in [10, 37]. Two images of the same area taken before and after the GB migration are subtracted. The nanoparticles on the sample surface are used as markers, the subtraction of both pictures is performed by the superimposing of markers in a given grain, here G_2. Because of the shear-migration coupling, the markers in grain G_1 do not superimpose: the markers appear with black and white contrasts. The relative displacements of the markers compared to grain G_2 are deduced from these contrasts. Figure 5(a),(b) and (c) provide the differences between Figure 4(b) and (a), between Figure 4(e) and (b) and between Figure 4(f) and (e), respectively.

As shown in Figure 1, the shear displacement is expected to depend linearly on the migration distance in the area swept by the GB migration, and is then constant above the GB.

The motion of the step s_1, characterized in Figure 5(a) is now detailed. The displacements of one marker noted x_1 located in the area swept by the GB and six markers noted x_2 to x_7 located above the area swept by the GB is indicated by arrows in Figure 5(a). The GB migration distance is m_1. As expected, the norms of displacements of x_2–x_7, noted d_2–d_7

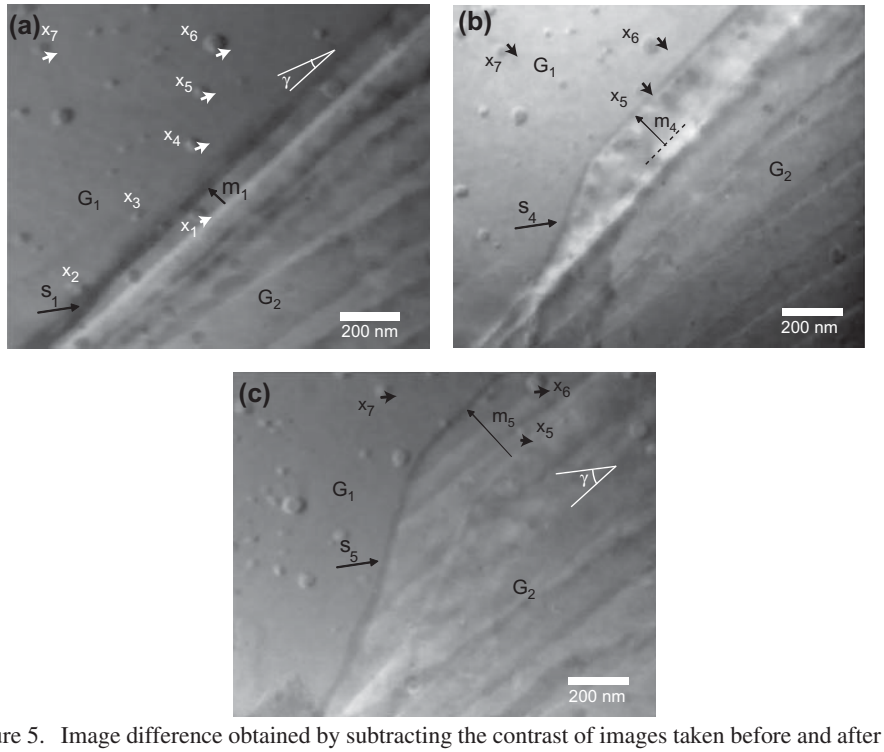

Figure 5. Image difference obtained by subtracting the contrast of images taken before and after the motion of step s_1 (a), s_4 (b) s_5 (c). When superimposing the markers in G_2, a shift in the markers position in G_2 is observed in all cases indicating that deformation has occurred. The coupling factor has both components parallel and perpendicular to the GB.

are equal, and their directions characterized by the angles γ_2–γ_7 between the displacement vector and the GB plane are also equal $\gamma_i = \gamma \approx 20^\circ$ (for $i = 1$ to 7). The coupling factor is deduced: $\beta_\parallel = \frac{d_i \cos\gamma}{m_1} \approx 25 \pm 2\%$. This coupling factor is close to the value obtained by macroscopic tests on the same bicrystals [12,35]. Besides, the migration of the step produces not only a shear strain (parallel to the GB plane) but also a displacement perpendicular to the GB plane. We characterize the markers, displacements perpendicular to the GB plane by the coefficient : $\beta_\perp = \frac{d_i \sin\gamma}{m_1} \approx 6 \pm 2\%$ ($i = 2$ to 7), corresponding to a deformation perpendicular to the GB.

Analyzing Figure 5(b), the coupling factor related to the motion of s_4 is estimated to be $\beta_\parallel \approx 0 \pm 2\%$ whereas the displacements perpendicular to the GB plane is characterized by $\beta_\perp = \frac{d_5 \sin\gamma}{m_4} = \frac{d_6 \sin\gamma}{m_4} \approx 6 \pm 2\%$.

Finally, Figure 5(c) related to the formation of the macro- step s_5 is considered. The displacement of three markers in G_1, two below the step (x_5 and x_6) and one above (x_7), are analysed. Again, the displacement of the markers is not purely parallel to the GB. Surprisingly, even in the area not swept by the step, markers displacement can also be noted. Moreover, the markers displacement profile in front of the step is similar to the one behind the step. An explanation of this observation is discussed in Section 4.3.

As expected, the markers displacement in the area swept by the GB is not constant but increases with the distance to the initial position of the GB (see Figure 1). The coupling

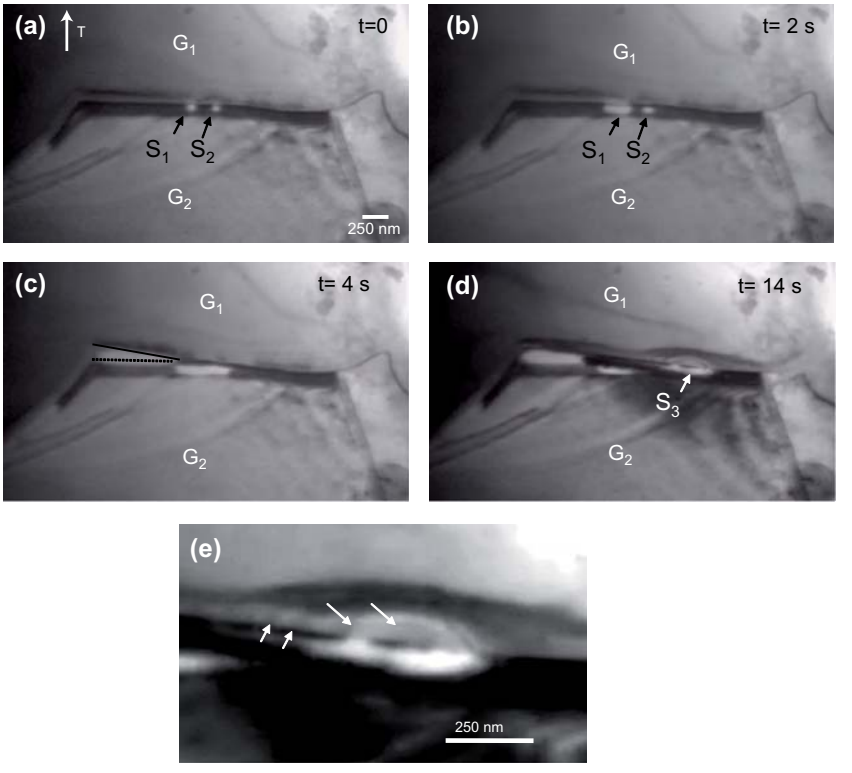

Figure 6. Sequence of bright field micrographs showing the emission of dislocation loops inside the GB in S_1 and S_2 (a-b) followed by a GB migration (c) in a polycrystal. (e) is a zoom of (d) showing the operation of the source S_3. Note in (e) the concentric dislocation loops noted by arrows emitted in G_1 and G_2.

factor due to the motion of s_5 can again be estimated $\beta_{\parallel} = \frac{d_7 \cos\gamma}{m_5} \approx 7 \pm 2\%$ and the analysis of the displacements perpendicular to the GB plane gives: $\beta_{\perp} = \frac{d_7 \sin\gamma}{m_5} \approx 6 \pm 2\%$.

The displacements perpendicular to the GB plane, observed in all analysed GB motions, were not expected from the analysis sketched in Figure 1: the motion of the step is supposed to involve climb processes, i.e. long-range diffusion, which are enabled by the high temperature. The interpretation of these phenomena will be discussed in detail in Section 4.1.

3.2. *GB Dislocation nucleation*

Figure 6 reports pictures taken during an *in situ* experiment in the Al polycrystal. The corresponding video is shown in the supplementary material section. A GB between two grains G_1 and G_2 is initially slightly inclined with respect to the foil surface and thus exhibits a uniform black and thick contrast. The straining axis (T) is indicated by an arrow in Figure 6(a). The time origin t = 0 s is defined when two bright contrasted points S_1 and S_2 appear along the GB (Figure 6(a)). They can be attributed to the nucleation of dislocation loops at two sources S_1 and S_2. The two loops eventually expand (Figure 6(b)) and finally impinge. In the meantime at time t = 4 s, a rapid GB migration is observed in the left part

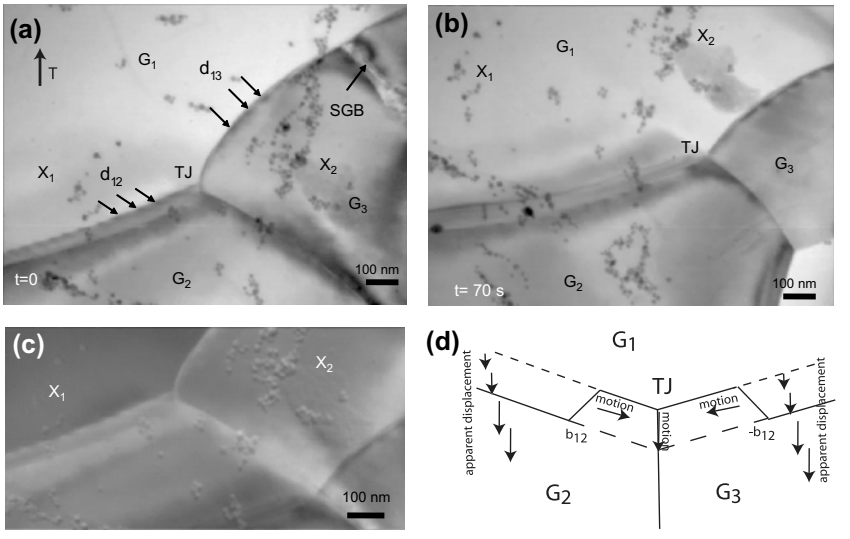

Figure 7. (a-b) Simultaneous deformation coupled migration of two GBs. Note the presence of GB dislocation d_{12} and d_{13} moving in opposite direction toward the GB during the GB migration. (c) The difference (a-b) with marker X_1 superimposed shows a shift in the markers in G_2 and G_3 (X_2 for instance). An apparent coupling factor around 5% is measured. The coupled motion is thought to occur as schematically drawn in (d).

of the GB (Figure 6(c)): the initial and final positions of the GB during this migration are respectively indicated by a dashed and a solid line.

Although, it was not possible to fully characterize these dislocation loops, this observation tends to indicate that a correlation exists between the nucleation of defects in the GB and the migration of the GB.

Shortly after (t = 14 s), another dislocation source noted S_3 appears in the right part of the GB as reported in Figure 6(d). Figure 6(e) is a zoom of the source S_3. Contrary to S_1 and S_2, it seems that several dislocation loops are emitted from S_3 in G_1 and G_2, indicating that intragranular plastic mechanisms can also be activated in addition to stress-assisted GB migration.

It is worth noting that macroscopic observations performed on Al bicrystals also revealed that the stress-induced moving boundaries can act as sources of lattice dislocations. These dislocations eventually lead to the generation and growth of new (sub)grains in the GB region [13,38].

3.3. *GB dislocation motion in polycrystals*

Figure 7 reports a more complex situation involving three grains G_1, G_2 and G_3, and the migrations of two GBs. In the following, the notation GB_{ij} refers to the GB between grains i and j. The experiment is reported in the video available in the supplementary material section. Figure 7 only reports some snapshots at judicious times. The straining axis (T) is indicated by an arrow in Figure 7(a). A $t = 0$ s, two trains of dislocations labelled d_{12} and d_{13} can be observed moving in opposite directions along the two high angle GBs, GB_{12} and GB_{13}. The dislocations d_{13} have been emitted at the junction between a subgrain boundary SGB and GB_{13}. At $t = 70$ s, both GB_{12} and GB_{13} have migrated about 400 nm,

corresponding to a mean migration speed of 10 nm/s. Figure 7(c) reports the difference between Figure 7(b) and 7(a), the markers in grain G_1 being superimposed. The analysis of Figure 7(c) shows that the markers displacements are approximately perpendicular to the GB_{12} and GB_{13} traces. However, since the GBs are inclined, part of the apparent displacement can have a shear component parallel to the GB but out of the plane of the image. Figure 7(c) also reveals that the markers displacement increases in the area swept by the GB with the distance from the initial position of the GB. From the measure of the displacements perpendicular to the GB, one gets an apparent coupling factor $\beta_a \approx 5\%$. It is interesting to note that the markers displacements are approximately the same in both grains G_2 and G_3, suggesting that the same coupling mechanism operates in both GBs. The GB migrations can be interpreted as follows (Figure 7(d)): in GB_{12}, step dislocations d_{12} of Burgers vector $\vec{b}_{12}$ move toward the triple junction (TJ in Figure 7(a) and (b)), leading to an apparent marker displacement deformation. In the meantime, in GB_{13}, step dislocations d_{13} with an opposite Burgers vector $\vec{b}_{13} = -\vec{b}_{12}$ move in the opposite direction, leading thus to the same deformation which produces the apparent displacement profile sketched in Figure 7(d). When the two-step dislocations meet at the GB, they annihilate and lead to the motion of the triple junction.

4. Discussion

The results of Section 3 evidence that stress driven GB migration in the investigated bicrystals and coarse grained polycrystals occurs at high temperature (i.e. $0.7\,T_m$) by the rapid and repeated motion of steps (Figure 3 and 4). Indeed, each time the step goes through the entire GB, it produces a GB migration over a distance equal to the step height. These steps are probably composed of nanometer height elementary steps as suggest by Sect. 3.1.1. These elementary steps carry a plastic deformation, i.e. the steps have a dislocation character [29,31]. This conclusion, proposed in interfacial dislocation model such as SMIG or DSC models, confirms that GB dislocation steps (disconnections) operate in high angle GBs similarly to their actions in twinning or martensitic transformation. In addition, the amount of produced deformation can be different from one step to another, suggesting that several kinds of GB dislocation steps can be responsible of the GB motion, or in other words, that a given GB can support several coupling modes. Thus, the coupling factor of a GB may depend locally on its defects rather than its macroscopic character.

In polycrystals where GBs are curved, the motion of the step can also be coupled to capillarity forces (see Figure 7). When capillarity forces are the only driving force, the GB migration is supposed to occur without deformation as it has been also observed experimentally [26,39], presumably by the pure shuffling mechanism.

4.1. *Step combination and coupling factor*

We propose in this paragraph to explain the former observations introducing a model involving the combination of steps of different heights and different Burgers vectors. These steps can also be considered as disconnections or group of disconnections.

Consider the motion of a first step, for instance the step s_a producing a pure shear parallel to the GB plane : a sketch of this situation is proposed in Figure 8(a). In this case, as already shown in Figure 1, the markers displacement profile linearly increases with the migration distance in the area swept by the GB migration, and is then constant above the GB.

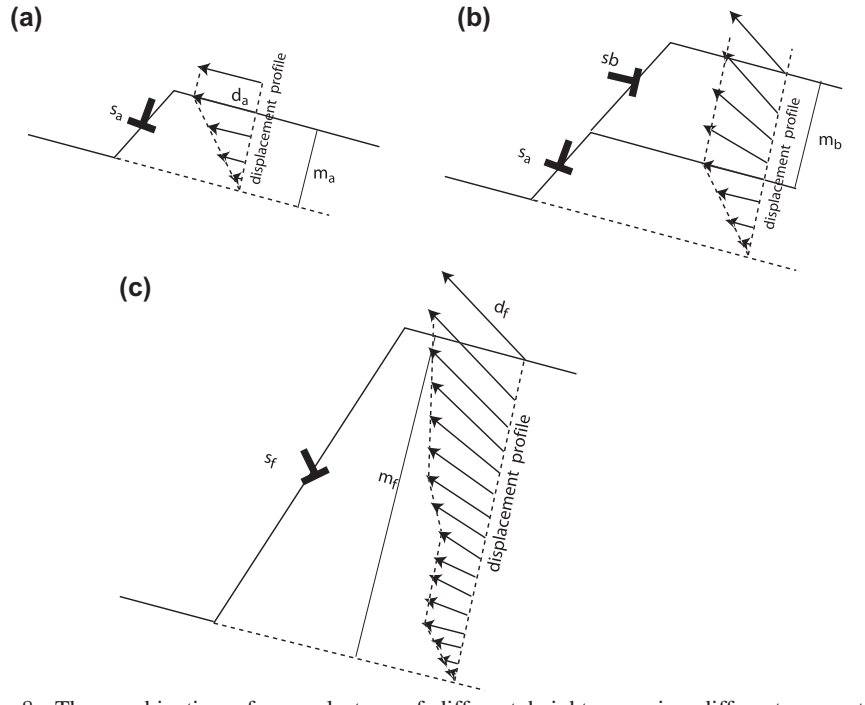

Figure 8. The combination of several steps of different heights carrying different amounts of deformation (a-b) is responsible for the observed final displacement profile (c).

If a second step s_b coupled to a strain perpendicular to the GB plane, stacks to the former step s_a, the displacement profile will be modified as shown in Figure 8(b). The total markers displacements induced by both steps s_a and s_b will be characterized by a coupling factor $\beta_{\parallel} = \frac{d_a}{m_a+m_b}$ and a coefficient $\beta_{\perp} = \frac{d_b}{m_a+m_b}$, where m_a and m_b are the s_a and s_b step heights and d_a and d_b are the strain carried by the steps.

If several steps of different heights carrying different amount of deformation (and not only shear) move along the GB and eventually pile up as sketched in Figure 8(c), the observed average coupling factor will be :

$$\langle \beta_{\parallel} \rangle = \frac{\sum_i d_i \cos \gamma_i}{\sum_i m_i} \tag{1}$$

and for the average coefficient $\beta_{\perp}$:

$$\langle \beta_{\perp} \rangle = \frac{\sum_i d_i \sin \gamma_i}{\sum_i m_i} \tag{2}$$

Where γ_i is the angle between the strain direction carried by the step and the GB plane.

This explanation will help us to interpret the markers displacement observed in the previously described experiments. Figure 9(a) shows the plot of the difference between Figure 4(f) and 4(a), superimposing the markers in grain G_2: it thus characterizes the displacement induced by the macro-step s_5. The displacement of seven markers x_i is analysed. Figures 9(b) and (c) plot the markers displacements respectively, parallel $d_{\parallel}$ and

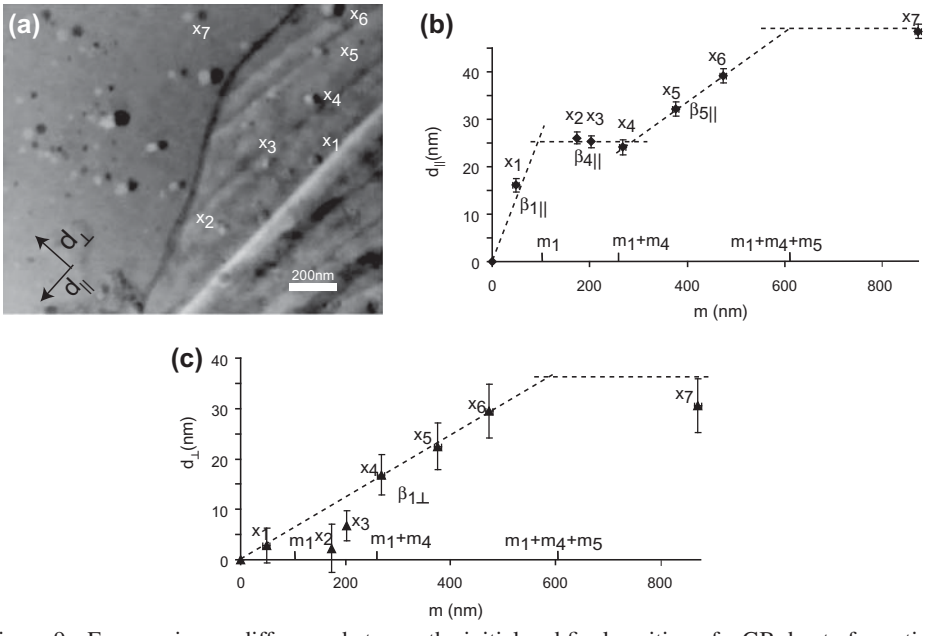

Figure 9. From an image difference between the initial and final position of a GB due to formation of the macro-step s_5 (a), the markers displacement profile parallel and perpendicular to the GB can be drawn (b) and (c). The different slopes in the curves correspond to the different coupling factors associated to the step motion.

perpendicular $d_\perp$ to the GB plane *vs.* their distances m from the initial position of the GB plane. In the first part of the curve corresponding to the motion of s_1, i.e. for $0 < m < m_1$, both curves $d_\parallel$ and $d_\perp$ show a linear increase with m. The respective slopes of these curves are $\beta_{\parallel 1} \approx 25\%$ and $\beta_{\perp 1} \approx 6\%$. These quantities are coherent with the coupling factor $\beta_\parallel$ and coefficient $\beta_\perp$ measured from Figure 5(a) i.e. from the displacements induced by step s_1 only.

For $m_1 < m < m_1 + m_4$, the curve $d_\parallel$ (Figure 9(b)) shows a plateau while $d_\perp$ (Figure 9(c)) linearly increases. The respective slope of these curves are $\beta_{\parallel 4} \approx 0\%$ and $\beta_{\perp 4} \approx 6\%$. These values are consistent with the coupling factors measured from Figure 5(b) while analysing the displacements induced by step s_4.

For $m_1 + m_4 < m < m_1 + m_4 + m_5$, both curves $d_\parallel$ and $d_\perp$ show a linear increase with slopes $\beta_{\parallel 5} \approx 6\%$ and $\beta_{\perp 5} \approx 6\%$. Again, this result is in agreement with the values found from Figure 5(c) while analysing the displacement induced by the steps forming the step s_5.

Since $\beta_{\perp 1} \approx \beta_{\perp 4} \approx \beta_{\perp 5}$, the curve $d_\perp$ (Figure 9(c)) does not show any slope change in the range $0 < m < m_1 + m_4 + m_5$.

For $m > m_1 + m_4 + m_5$, both the parallel and perpendicular displacement $d_\parallel$ and $d_\perp$ present a plateau : see marker x_7 in Figure 9(b) and (c). They correspond to the overall displacements induced by the set of steps s_1 to s_4, or equivalently by the macro-step s_5.

Finally, the overall coupling factor $\langle \beta_\parallel \rangle$ and coefficient $\langle \beta_\perp \rangle$ can be retrieved from these curves according to Equation 1 and 2: $\langle \beta_\parallel \rangle \approx 6.8\%$ and $\langle \beta_\perp \rangle \approx 6.4\%$.

4.2. *GB dislocation step origin*

Some elementary GB dislocation steps were found prior to deformation and were probably inherent defects in the structure of the GB itself. However, because GB steps are deeply related to the GB migration under stress, they have to be nucleated at a certain rate as the GB migrates. Intrinsic GB sources have been observed (see Figure 6) during their operation. Atomistic simulations have also shown the nucleation and expansion of a disconnection loop in a GB to account for the shear response of a tilt GB in Ni [40], and disconnection sources have also been identified in $\{10\bar{1}2\}$ twin in HCP metals [41]. GB dislocations can also be nucleated from a sub-grain boundary intersecting a GB (Figure 7). Although the detailed nucleation mechanism is unknown, the operation of a source can take its origin from a spiral source formed by lattice dislocations trapped in a GB. Indeed, a GB dislocation of Burgers $\vec{b}_s$ can result from the interaction between two lattice dislocations of Burgers vector $\vec{b}_1$ and $\vec{b}_2$ according to: $\vec{b}_s = \vec{b}_1 + \vec{b}_2$. If the two lattice dislocations are sessile, they can act as a fixed arm around which the GB dislocation can spin under the shear stress [42]. Every turn, a GB dislocation is nucleated. Such a source cannot however last since the GB migrates perpendicularly in the meantime.

4.3. *Step motion and pinning and intragranular plasticity*

Steps have been frequently found to be pinned by localized obstacles during their motion. Because steps cannot pass each other, the accumulation of elementary GB dislocation steps on a pinning point forms the observed macro-steps. Some of these steps like the step s_1 can produce a large amount of deformation as observed in macroscopically deformed bicrystalline samples [12,13,35,36].

However, in contrast to these cited studies where the tensile stress is maintained below the elastic limit, the control of both the intensity and the homogeneity of the applied stress level is difficult in our TEM experiments: an intragranular plastic stress relaxation may hence occur.

GB dislocation steps have been shown to be frequently impeded by obstacles during their motion. These obstacles can be some defects of the GB structure, like lattice dislocations trapped in the GB, or can be related to a defect at the sample surface. This latter type of obstacles is expected to play a crucial role for the step motion in TEM thin foils. The blocking of the steps prevents the propagation of the deformation (Figure 10(a)). Because steps are supposed to be composed by several elementary GB dislocation steps, they probably develop a large long-range stress/strain field. When permanently blocked, this stress/strain field may relax through intergranular plasticity.

This situation may explain why the markers displacements, i.e. the deformation profile perpendicular to the GB, observed below and in front of the final step s_f in Figure 5 are similar. Indeed, when the GB dislocation steps of Burgers vector $\vec{b}_s$ are stopped, the shear can be efficiently transferred in front of the step in G_1 by the glide in different planes of lattice dislocations of Burgers vector $\vec{b}_{11}$ and $\vec{b}_{12}$ as schematically represented in Figure 10(b). In this case, these dislocations are supposed to be nucleated inside G_1. This mechanism is supported by the observation of a plastic deformation in front of the step in Figure 4(g).

The interaction between lattice dislocations from G_1 and GB dislocations can lead to the decomposition of the GB dislocation step and to the formation of lattice dislocations

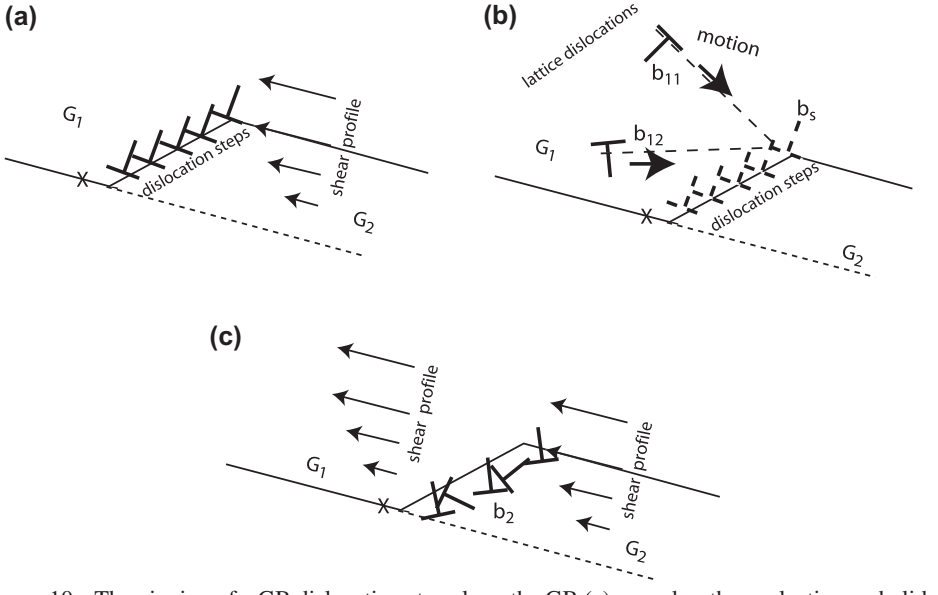

Figure 10. The pinning of a GB dislocation step along the GB (a) provokes the nucleation and glide of lattice dislocations in front of the step in order to release the strain produced by the shear-coupled motion (b). The lattice dislocation glide propagates the shear strain in front of the step. The interaction between lattice dislocations and GB dislocations produces dislocations in G_2. This may leave the step with a lower dislocation content (c).

in G_2 according to $\vec{b}_s = \sum_i \vec{b}_{1i} + \sum_j \vec{b}_{2j}$. This decomposition may thus lead to a less energetic step and ultimately to a pure step with no dislocation (Figure 10(c)).

This interpretation is similar to the theory of emissary slip developed by Sleeswyk [43] to explain the plastic accommodation in front of a growing twin. In this theory, the very high stress and strain produced in the vicinity of a deformation twin can be relaxed by the decomposition of a twin dislocation into a slip dislocation (an emissary dislocation) that is eventually emitted in front of the twin and a so-called complementary twin partial. Emissary dislocations have been observed in various metals as reported in [44].

4.4. *Step mobility*

The very fast step motion suggests that the GB mobility is controlled not only by the propagation of the GB dislocation step itself but also by the nucleation of the GB dislocation steps and their pinning by defects along the GB. Such pinning has already been found to decrease the mobility of pure tilt GBs during recrystallization processes [45]. However, little is known about the energy required to nucleate such GB dislocation steps.

In contrast, the mobility of disconnections has been extensively discussed in the general case in [14]. As revealed by computer simulations, for twins, the motion of GB dislocations step with small Burgers vectors and small step height is favoured [41]. Indeed, long-range elastic strains decrease when Burgers vectors are small, and less shuffled atoms are implied when the step height is small.

However, GB dislocation steps with smaller Burgers vector and/or larger step height, i.e. leading to smaller coupling factor, are also probably mobile with the help of the thermal

activation when small strains have to be achieved in order to reduce strain incompatibilities in polycrystals. The present study reports also that the dislocation step can carry a significant climb component (Figure 5(c) and (d)) which also implies long-range diffusion processes that are strongly thermally activated. Interesting implications can be deduced from the simulations by Mishin et al. [46,47] who investigated the dynamics of GB migration coupled to shear and showed that GBs respond to stress by a stick-slip behaviour, which is a typical deformation mechanism caused by a Peierls potential. We may speculate that the energy required to nucleate and propagate a pair of GB dislocation steps is mainly related to such a Peierls potential. We can assume that it depends on both the step height and the germ width, i.e. the lateral extension of a critical pair of GB dislocation steps. It can be assumed that the germ width will be smaller when the lattice periodicity along the GB is smaller, i.e. for low Σ coincident GB. Then, the Peierls potential is thus believed to be smaller for misorientation angles close to low Σ values, in agreement with the misorientation dependence of the measured activation enthalpy of the stress-driven GB migration in Al bicrystals [12].

5. Conclusions

The results presented in this paper lead to the following conclusions:

- Shear-coupled GB migration has been observed in Al bi- and poly-crystals at 400 ° C.
- the GB migration occurs through the nucleation and the propagation of steps along the GB.
- These steps carry a plastic deformation, i.e. the steps are GB dislocation steps (also called disconnections) [29,31].
- A migrating GB can support different GB dislocation steps, each of them producing their particular deformation.
- Especially, the deformation can have a component perpendicular to the GB plane.
- In polycrystalline Al, the collective motion and annihilation of these step dislocations are supposed to account for GB stress assisted migration.

These results, which highlight the complexity of stress-assisted GB migration mechanisms, indicate the difficulty to predict coupling modes by a purely geometrical approach. It also gives a completely different perspective on coupling motion. Locally, at the nanoscale, the deformation produced by such a mechanism is dependent on the nucleation and propagation of several kind of GB defects, in which density can vary from one part of the GB to another. Macroscopically, however, the collective motion of GB step dislocations may lead to a coupling factor representing an average value over all possible elementary coupling factors. The identification of elementary defects in the GB will be the purpose of a future study.

Acknowledgements

The authors acknowledge D. Caillard and S. Lartigue for fruitful discussions and are grateful to J.E. Brandenburg and D. Lamirault for assistance in bicrystal growth and sample preparation. One of the authors (DM) expresses his gratitude to the Deutsche Forschungsgemeinschaft for financial support (Grant MO 848/14-1).

References

[1] D.S. Gianola, S. Van Petegem, M. Legros, S. Brandstetter, H. Van Swygenhoven and K.J. Hemker, Acta Mater. 54 (2006) p.2253.
[2] M. Legros, D. Gianola and K. Hemker, Acta Mater. 56 (2008) p.3380.
[3] T.J. Rupert, D.S. Gianola, Y. Gan and K.J. Hemker, Science 326 (2009) p.1686.
[4] C.H. Li, E.H. Edwards, J. Washburn and E.R. Parker, Acta Metall. 1 (1953) p.223.
[5] D.W. Bainbridge, C.H. Li and E.H. Edwards, Acta Metall. 2 (1954) p.322.
[6] J. Christian *The Theory of Transformations in Metals and Alloys*, Pergammon, Oxford, 2002.
[7] S.E. Babcock and R.W. Balluffi, Acta Metall. 37 (1989) p.2357.
[8] H. Fukutomi, T. Iseki, T. Endo and T. Kamijo, Acta Metall. Mater. 39 (1991) p.1445.
[9] A.D. Sheikh-Ali, Acta Mater. 58 (2010) p.6249.
[10] F. Mompiou, D. Caillard and M. Legros, Acta Mater. 57 (2009) p.2198.
[11] F. Mompiou, M. Legros and D. Caillard, MRS symp. proc. 1086-U09-04 (2008).
[12] T. Gorkaya, D.A. Molodov and G. Gottstein, Acta Mater. 57 (2009) p.5396.
[13] D.A. Molodov, T. Gorkaya and G. Gottstein, Journal Mater. Sci. 46 (2011) p.4318.
[14] R.C. Pond and S. Celotto, Int. Mat. Revs. 48 (2003) p.225.
[15] A. Sutton and R. Baluffi, *Interfaces in Crysalline Materials*, Oxford University Press, Oxford, 1995.
[16] J.W. Cahn and J.E. Taylor, Acta Mater. 52 (2004) p.4887.
[17] J.W. Cahn, Y. Mishin and A. Suzuki, Acta Mater. 54 (2006) p.4953.
[18] J. Schafer and K. Albe, Acta Mater. 60 (2012) p.6076.
[19] C.M.F. Rae and D.A. Smith, Phil. Mag. A 41 (1980) p.477.
[20] D. Caillard, M. Legros and F. Mompiou, Acta Mater. 57 (2009) p.2390.
[21] F. Mompiou, M. Legros and D. Caillard, Acta Materialia 58 (2010) p.3676.
[22] W. Read and W. Shockley *Imperfections in Nearly Perfect Crystals*, Mac Grawth Hill, New York, 1957.
[23] Z.T. Trautt, A. Adland, A. Karma and Y. Mishin, Acta Mat. 60 (2012) p.6528.
[24] A. Suzuki and Y. Mishin, Mater. Sci. Forum 502 (2005) p.157.
[25] R.C. Pond, X. Ma, Y.W. Chai and J.P. Hirth *Dislocations in Solids*, Vol. 13, Elsevier, Amsterdam, 2007.
[26] S.E. Babcock and R.W. Balluffi, Acta Metall. 37 (1989) p.2367.
[27] J. Hirth, Acta Metall. 22 (1974) p.1023.
[28] M. Guilloppe and J. Poirier, Acta Metall. 28 (1980) p.163.
[29] F. Mompiou, M. Legros and D. Caillard, Acta Mat. 58 (2010) p.3676.
[30] C. Wayman *Introduction to the Crystallography of Martensitic Transformations*, Macmillan, 1964.
[31] J.P. Hirth and R.C. Pond, Acta Mater. 44 (1996) p.4749.
[32] H.A. Khater, A. Serra, R.C. Pond and J.P. Hirth, Acta Materialia 60 (2012) p.2007.
[33] D.A. Molodov, T. Gorkaya and G. Gottstein, Script. Mater. 65 (2011) p.990.
[34] T. Gorkaya, K.D. Molodov, D.A. Molodov and G. Gottstein, Acta Mater. 59 (2011) p.5674.
[35] D.A. Molodov, V.A. Ivanov and G. Gottstein, Acta Mater. 55 (2007) p.1843.
[36] D.A. Molodov, T. Gorkaya and G. Gottstein, Mater. Sci. Forum 558–559 (2007) p.927.
[37] F. Mompiou, M. Legros and D. Caillard, J. Mater. Sci. 46 (2011) p.4308.
[38] D.A. Molodov, T. Gorkaya and G. Gottstein, Mater. Sci. Forum 715–716 (2012) p.227.
[39] F. Mompiou, M. Legros, T. Radetic, U. Dahmen, D. Gianola and K. Hemker, Acta Mater. 60 (2012) p.2209.
[40] L. Wan and S. Wang, Phys. Rev. B 82 (2010) p.214112.
[41] A. Serra and D. Bacon, Phil. Mag. A 73 (1996) p.333.
[42] F. Mompiou, M. Legros, A. Sedlmayr, D. Gianola, D. Caillard and O. Kraft, Acta Materialia 60 (2012) p.977.

[43] A.W. Sleeswyk, Acta Metall. 10 (1962) p.803.
[44] S. Mahajan and G.Y. Chin, Acta Metall. 22 (1974) p.1113.
[45] D.A. Molodov, P. Konijnenberg, W. Hu, G. Gottstein and L.S. Shvindlerman, Scripta Materialia 45 (2001) p.229.
[46] Y. Mishin, A. Suzuki, B. Uberuaga and A. Voter, Phys. Rev. B 75 (2007) p.224101.
[47] V. Ivanov and Y. Mishin, Phys. Rev. B 78 (2008) p.064106.